Journal of Power Sources 232 (2013) 12–16

Contents lists available at SciVerse ScienceDirect

Journal of Power Sources

journal homepage: www.elsevier.com/locate/jpowsour

Short communication

Acetylene black-embedded $LiMn_{0.8}Fe_{0.2}PO_4$/C composite as cathode for lithium ion battery

B.Z. Li [a], Y. Wang [a], L. Xue [a], X.P. Li [a,b,c], W.S. Li [a,b,c,*]

[a] School of Chemistry and Environment, South China Normal University, Guangzhou 510006, China
[b] Key Laboratory of Electrochemical Technology on Energy Storage and Power Generation of Guangdong Higher Education Institutes, South China Normal University, Guangzhou 510006, China
[c] Engineering Research Center of Materials and Technology for Electrochemical Energy Storage (Ministry of Education), South China Normal University, Guangzhou 510006, China

HIGHLIGHTS

- A novel $LiMn_{0.8}Fe_{0.2}PO_4$/C composite was synthesized by a simple sol–gel method.
- Acetylene black as carbon source was embedded in $LiMn_{0.8}Fe_{0.2}PO_4$.
- The composite exhibits superior rate capability as cathode of Li-ion battery.

GRAPHICAL ABSTRACT

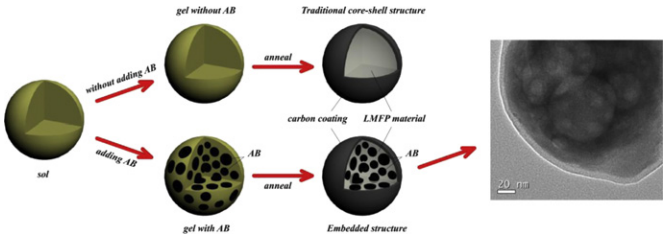

ARTICLE INFO

Article history:
Received 8 October 2012
Received in revised form
2 January 2013
Accepted 3 January 2013
Available online 12 January 2013

Keywords:
Lithium ion battery
Embedded structure
Lithium manganese iron phosphate
Acetylene black

ABSTRACT

A novel $LiMn_{0.8}Fe_{0.2}PO_4$/C composite is synthesized *via* a sol–gel process. In this composite, acetylene black is embedded in $LiMn_{0.8}Fe_{0.2}PO_4$. The structure and morphology of the resulting composite are characterized with XRD, SEM, TEM, and BET, and its performance as the cathode of lithium ion battery is investigated by charge–discharge test and EIS, with a comparison of the sample prepared without embedding acetylene black. It is found that the embedded composite exhibits better performance than the non-embedded sample. The former delivers a reversible capacity of 160 mAh g^{-1}, while the latter only 142 mAh g^{-1} at 0.1 C (1C = 150 mAh g^{-1} in the work). The embedded acetylene black not only functions as a barrier for the growing of $LiMn_{0.8}Fe_{0.2}PO_4$ particles in the preparation process, which is important for the formation of nano-particles, but also helps build a stable conductive network, thus improving the charge–discharge performance of $LiMn_{0.8}Fe_{0.2}PO_4$.

1. Introduction

Olivine $LiFePO_4$ has been well studied as a cathode material for safe lithium ion battery due to its structural stability [1–5]. However, the potential of $LiFePO_4$ is too low (3.5 V vs. Li^+/Li) to meet the requirement of high energy density in many applications such as electric vehicle. Alternatively, olivine $LiMnPO_4$ is attracting intensive attention because of its higher potential (4.0 V vs. Li^+/Li) [6–12]. Similarly to $LiFePO_4$, $LiMnPO_4$ has low ionic and electronic conductivity. Fortunately, these drawbacks can be overcome by iron doping and carbon coating [12–15]. In the case of Fe doping, the replacement of 20 at.% Mn in $LiMnPO_4$ ($LiMn_{0.8}Fe_{0.2}PO_4$) yields the best improvement [12].

To obtain a satisfactory performance of the olivine compounds as cathode materials of lithium ion battery, many structures have been constructed, such as core-shell [16,17], carbon-nanocomposite [6,18], micro-nano composite [19], and porous particle [20,21]. Among these structures, porous particle is found to be most effective in performance improvement of olivine due to its large contact surface area and 3D conductive network [20–22]. However, the performance of the cathode is tightly related to the pore size in

* Corresponding author. School of Chemistry and Environment, South China Normal University, Guangzhou 510006, China. Tel./fax: +86 020 39310256.
E-mail address: liwsh@scnu.edu.cn (W.S. Li).

0378-7753/$ – see front matter © 2013 Elsevier B.V. All rights reserved.
http://dx.doi.org/10.1016/j.jpowsour.2013.01.019

the olivine particles. Big pores lack the structure stability and reduce the loading of active material [20], while small pores do not favor the electrolyte penetration due to the large surface tension.

In this work, we developed a novel $LiMn_{0.8}Fe_{0.2}PO_4$/C composite by introducing porous acetylene black (AB) into the bulk of $LiMn_{0.8}Fe_{0.2}PO_4$. The embedded porous carbon provides not only the electronic conductive network due to the good electronic conductivity of AB, but also the ionic paths due to its porous structure and good compatibility with electrolyte, and the improved performance of $LiMn_{0.8}Fe_{0.2}PO_4$ as cathode of lithium ion battery can be expected.

2. Experimental

2.1. Sample preparation

AB-embedded $LiMn_{0.8}Fe_{0.2}PO_4$/C (LMFP-AB/C) was prepared *via* a sol–gel process as follows. $C_6H_8O_7\cdot H_2O$ (citric acid), $Mn(CH_3COO)_2\cdot 4H_2O$, $FeC_2O_4\cdot 2H_2O$, $LiCH_3COO\cdot 2H_2O$, $NH_4H_2PO_4$ (in a mole ratio of 1.20: 0.80: 0.20: 1.05: 1.00) and ethylene glycol were dissolved in 1.0 M HCl solution. 20 wt% of AB (Nippon Carbon Co., Ltd., Special type for Li-ion batteries) was added into the resulting solution, and a black gel was formed by the following heat at 90 °C. The AB content used in this work was based on the optimized content of AB for the preparation of a carbon-$LiMnPO_4$ composite by Sun et al. [6]. The gel was heated at 400 °C for 5 h and then at 800 °C for 15 h in Ar/H_2 (8%) to get final product. The sample with core-shell structure (LMFP/C) was also prepared for comparison in the same way but without adding AB. All the chemicals (except for AB) were analytical grade and purchased from Aladdin Reagent Co., Ltd. (Shanghai, China). The formation process of the samples is presented schematically in Fig. 1.

2.2. Physical and electrochemical characterizations

The carbon contents of the final products were estimated by TGA (TG Perkin–Elmer TGA7). The temperature for TGA ranged from 25 °C to 800 °C at a heating rate of 10 °C min^{-1} under oxygen atmosphere. The obtained results were 33 wt % for LMFP-AB/C and 16 wt % for LMFP/C. The carbon in LMFP-AB/C may not be detected if it is fully encapsulated in $LiMn_{0.8}Fe_{0.2}PO_4$. But this situation hardly happens because $LiMn_{0.8}Fe_{0.2}PO_4$ will decompose into Li_3PO_4 and Fe_2O_3 and the embedded AB will be exposed in TGA process.

The crystal structure of prepared materials was characterized by Powder XRD (Bruker D8 Advance Germany) with monochromated Cu-Kα radiation. The specific surface area and the pore-size distribution were determined with BET (Micromeritics ASAP 2020 M) at liquid nitrogen temperature (77 K). The particle size and morphology of the samples were observed by using the scanning electron microscopy (JEOL JSM-6380LA) and the transmission electron microscopy (JEOL JEM-2100HR).

The LMFP-AB/C electrode was composed of the active material LMFP-AB/C and polyvinylidene difluoride (PVDF) in a weight ratio of 9:1 (without adding any conductive carbon materials). The LMFP/C electrode was composed of the active material LMFP/C, AB and PVDF in a weight ratio of 7:2:1. The comparison of two electrodes could be considered to be equivalent, because the content of $LiMn_{0.8}Fe_{0.2}PO_4$ in both electrodes is about 60 wt%. The final loading of materials on both electrodes was about 3 mg cm^{-2}. The electrochemical measurements were conducted on a lithium coin-cell (CR2025). The electrolyte was 1 M $LiPF_6$ in ethylene carbonate (EC) and dimethyl carbonate (DMC) (1:1 in volume, Samsung) and the separator was Celgard 2300.

Charge–discharge test was carried out on a multi-channel battery tester (LAND CT2001A) at 25 °C. For the determination of C-rate performance, the cell was charged at a constant charge current of 0.05 C (1 C = 150 mAh g^{-1}) to 4.8 V, then discharged to 2.0 V at n C-rate (n = 0.1, 0.2, 0.5, 1, 2 and 5). For the determination of cyclic performance, the cell was charged at a constant charge current of 0.1 C–4.8 V, then discharged to 2.0 V at 0.05 C. Electrochemical impedance measurements of the fresh and cycled cells were performed using Autolab (PGSTAT302N) with AC signal of 10 mV_{rms} from 1 M Hz to 1 m Hz. For the measurement of the cycled cells, the cell was charged and discharged for 15 cycles at 0.1 C between 2.0 and 4.8 V.

3. Results and discussion

3.1. Structure and morphology

XRD was used to determine the crystal structure of the prepared samples. Fig. 2 presents the XRD patterns of LMFP-AB/C and LMFP/C, compared with that of AB. It can be found that the XRD patterns of both LMFP-AB/C and LMFP/C samples are similar. The sharp peaks indicate the good crystallization of the samples. No peak for impurities is found, suggesting that the $LiMn_{0.8}Fe_{0.2}PO_4$ samples are pure solid solution phase. The cell parameters of LMFP-AB/C obtained by Jade 5.0 are: a = 6.0812(3) Å, b = 10.4233(6) Å, c = 4.7320(4) Å, and V = 299.94 $Å^3$, which are consistent with those reported by Martha et al. [12]. It can be noted from the circle on the XRD pattern of LMFP-AB/C that the AB added during sol–gel process remains in the product after heating at 800 °C.

The morphology of the prepared samples was observed by SEM and TEM. Fig. 3 shows the SEM and TEM images of LMFP-AB/C and

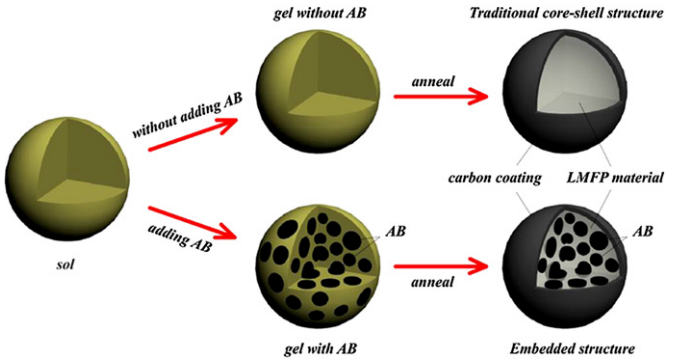

Fig. 1. Schematic formation processes of core-shell and embedded $LiMn_{0.8}Fe_{0.2}PO_4$/C composites.

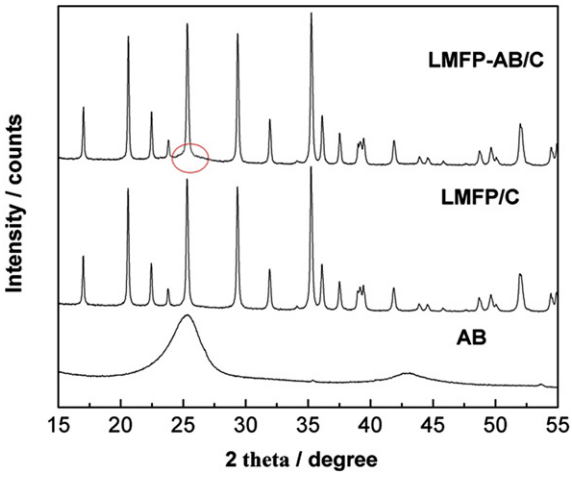

Fig. 2. XRD patterns of AB, LMFP/C and LMFP-AB/C (the difference between LMFP/C and LMFP-AB/C is indicated by a circle).

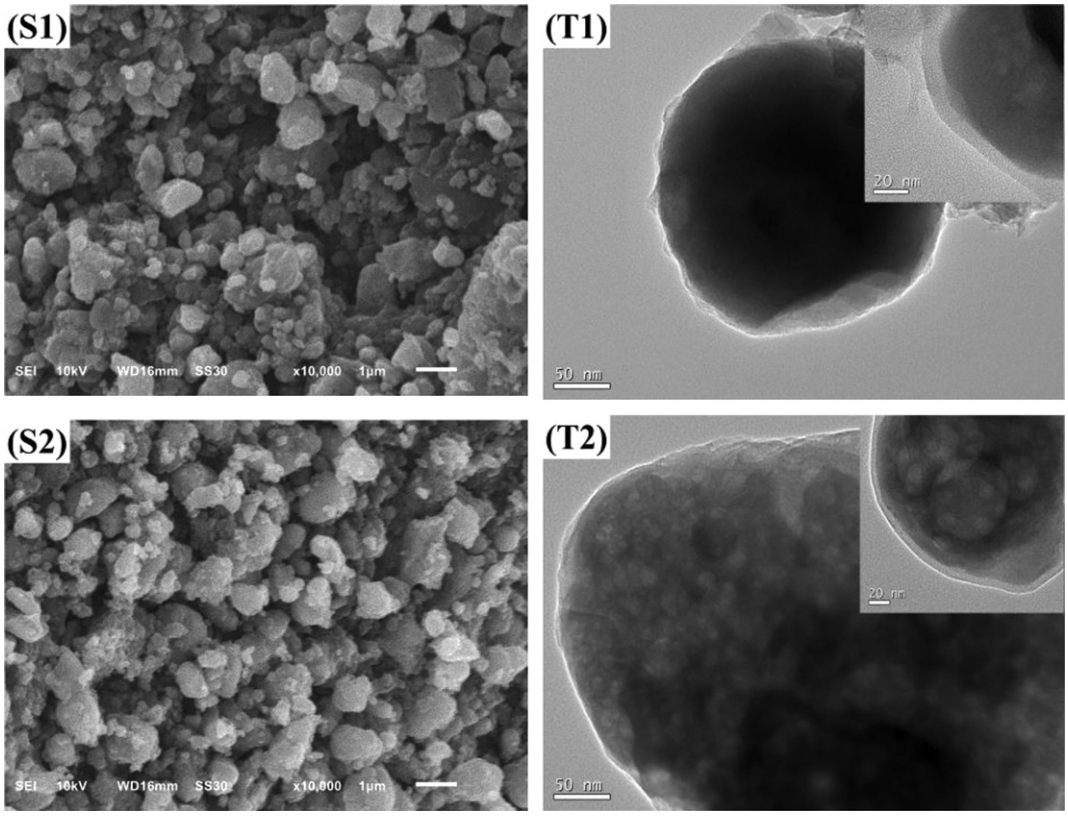

Fig. 3. SEM and TEM images of LMFP/C (**S1**, **T1**) and LMFP-AB/C (**S2**, **T2**).

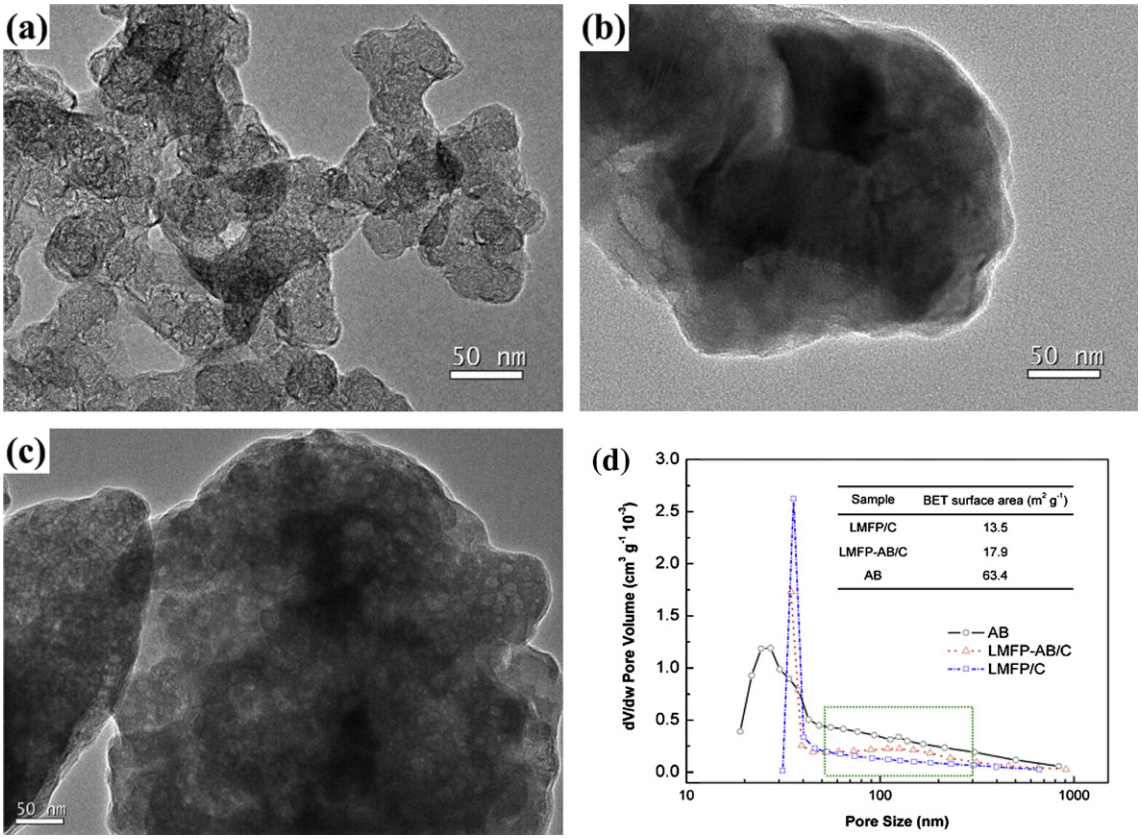

Fig. 4. TEM images of AB (a), precursor (the gel after treatment at 400 °C) of LMFP/C (b) and LMFP-AB/C (c), and pore-size distribution and specific surface area (d) of LMFP/C, LMFP-AB/C and AB (the difference between LMFP/C and LMFP-AB/C is indicated by a rectangle).

LMFP/C. It can be seen from the SEM images that the particle size and morphology of the both samples are similar, showing a well-distributed micro-nano structure. The primary particle size is in the range of 80–100 nm, which is reunited into the secondary particles of 1–2 μm. The micro-nano structure could not only improve the electrochemical performance but also enhance the tap density of the materials [19]. Although both samples have similar SEM images (Fig. 3 (**S1**) and (**S2**)), their TEM images are very different. The particle of LMFP/C sample has a core–shell structure, as shown in Fig. 3 (**T1**). Its particle size is about 200 nm with a uniform carbon layer of about 10 nm thick, which is similar to that prepared with a common sol–gel method [16]. However, the LMFP-AB/C has an embedded structure padded with AB balls, as shown in Fig. 3 (**T2**). This embedded structure is completely different from the porous structure reported by Wang et al. [21]. There is not any solid conductive material in the pore of their $Li_3V_2(PO_4)_3$. In our sample, the AB balls with particle sizes of 10–60 nm are embedded uniformly in $LiMn_{0.8}Fe_{0.2}PO_4$. It is apparent that the growing of $LiMn_{0.8}Fe_{0.2}PO_4$ particles can be inhibited by the use of AB and the resulting primary particles of $LiMn_{0.8}Fe_{0.2}PO_4$ should be far smaller than those of the LMFP/C sample. It can be noted from Fig. 3 (**T2**) that some unfilled pores in LMFP-AB/C particles were formed, which might be caused by the blind or small pores without filling the preparation solution in AB.

To confirm the embedded structure of LMFP-AB/C, the morphologies of AB and precursor (the gel after treatment at 400 °C) of LMFP/C and LMFP-AB/C were observed with TEM, and the specific surface area and pore size distribution of AB, LMFP/C and LMFP-AB/C were determined with BET and BJH. The obtained results are presented in Fig. 4. It can be seen from Fig. 4(a) that AB is composed

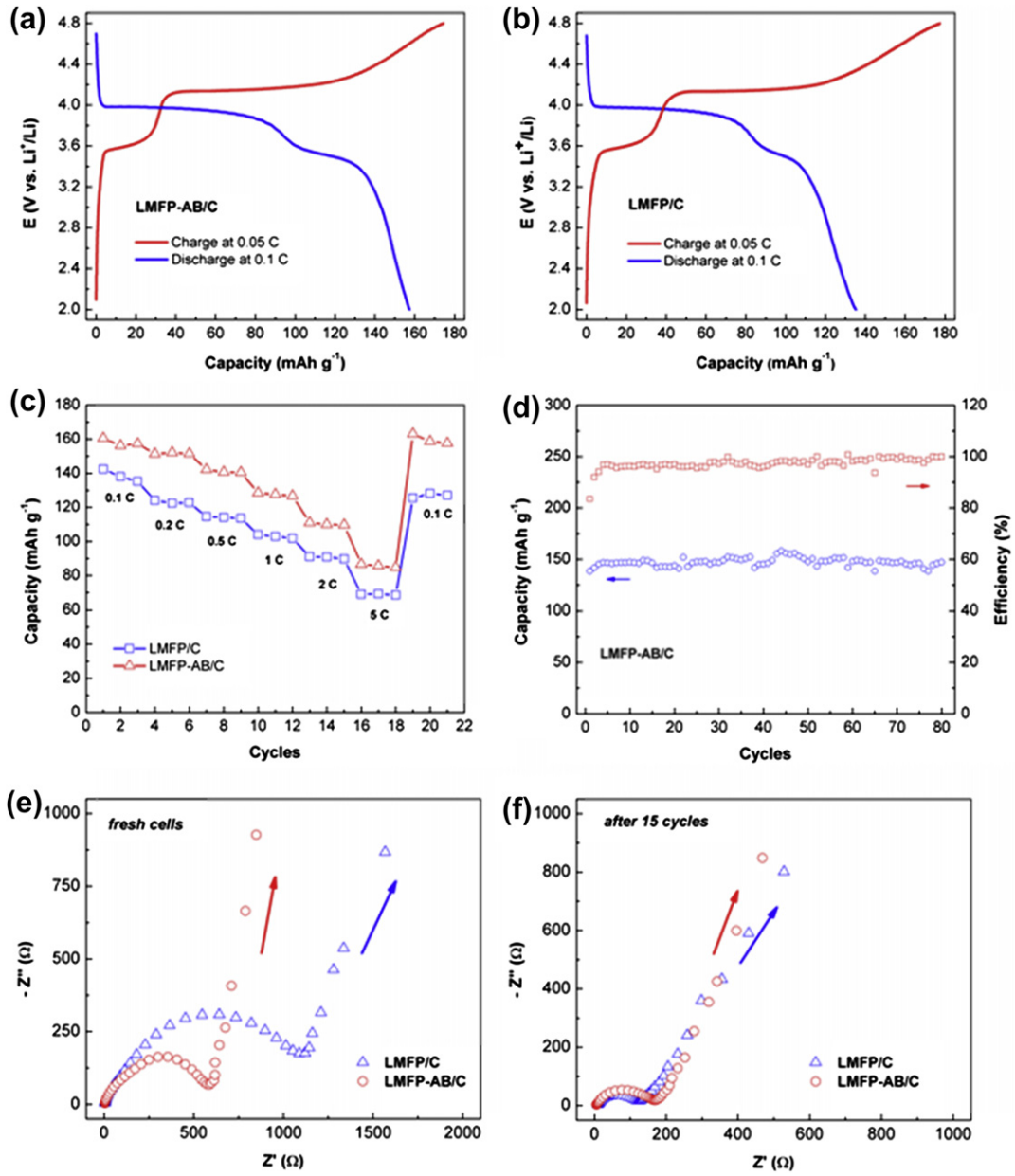

Fig. 5. Charge–discharge curves of LMFP-AB/C (a) and LMFP/C (b), charged to 4.8 V at 0.05 C and discharged to 2.0 V at 0.1 C; comparison of C-rate capability between LMFP-AB/C and LMFP/C (c); cyclic stability of LMFP-AB/C (d), charged to 4.8 V at 0.1 C and discharged to 2.0 V at 0.05 C; and electrochemical impedance spectra of the cells before cycling (e) and after 15 cycles (f) at open circuit voltage (3.0 V).

of the agglomerated particles of 20–40 nm. Compared with Fig. 4(b), Fig. 4(c) retains the morphology of AB, showing that AB has been successfully embedded in the LMFP-AB/C precursor. The difference in particle size distribution and specific surface area between LMFP-AB/C and LMFP/C can be seen from Fig. 4(d). AB has a broad pore size distribution from 20 to 200 nm, mainly in range of 20–40 nm, and has a large surface area (63.4 $m^2\ g^{-1}$). LMFP-AB/C has a larger specific surface area (17.9 $m^2\ g^{-1}$) than LMFP/C (13.5 $m^2\ g^{-1}$) and retains the pore size distribution of AB from 50 to 200 nm. These results confirm the contribution of AB to the porous structure of LMFP-AB/C.

Due to the porosity and the electronic conductivity of AB, the embedded structure of LMFP-AB/C provides not only the electronic conductive network but also the ionic paths, and the improved performance of $LiMn_{0.8}Fe_{0.2}PO_4$ as cathode material of lithium ion battery can be expected.

3.2. Electrochemical performance

The electrochemical performance of the prepared samples was understood by charge–discharge test. Fig. 5 presents the obtained results. The charge–discharge curves of LMFP-AB/C (Fig. 5(a)) and LMFP/C (Fig. 5(b)) show that both samples have similar charge–discharge characteristics. The two discharge potential plateaus at about 4.0 V and 3.5 V (vs. Li^+/Li) can be identified for both sample, corresponding to Mn^{3+}/Mn^{2+} and Fe^{3+}/Fe^{2+}, respectively [12]. It can be found that LMFP-AB/C delivers larger discharge capacity than LMFP/C. This difference can also be observed when the samples were discharged at other C-rates, as shown in Fig. 5(c). The reversible capacity is about 160 mAh g^{-1}, 152 mAh g^{-1}, 141 mAh g^{-1}, 128 mAh g^{-1}, 110 mAh g^{-1}, and 86 mAh g^{-1} for LMFP-AB/C, while only 142 mAh g^{-1}, 123 mAh g^{-1}, 114 mAh g^{-1}, 103 mAh g^{-1}, 91 mAh g^{-1}, and 69 mAh g^{-1} for LMFP/C at 0.1 C, 0.2 C, 0.5 C, 1 C, 2 C and 5 C, respectively. These results indicate that LMFP-AB/C exhibits better performance as cathode material of lithium ion battery than LMFP/C. Compared with the $LiMn_{0.8}Fe_{0.2}PO_4$/C composite developed by Hu et al. ($\sim$80 mAh g^{-1} at 0.1 C) [23], it can be noted that prepared process of LMFP/C composite is important for the discharge performance improvement of $LiMn_{0.8}Fe_{0.2}PO_4$. After cycled at different C-rates (from 0.1 to 5 C), both samples did not reduce their primary capacity, 163 mAh g^{-1} for LMFP-AB/C and 126 mAh g^{-1} for LMFP/C at 0.1 C, showing the structure stability of the prepared samples. To further confirm the stability of the embedded structure, the cyclic performance of the LMFP-AB/C was determined by charging to 4.8 V at 0.1 C and discharging to 2.0 V at 0.05 C. The obtained result is shown in Fig. 5(d). The charge–discharge efficiency is higher than 95% and the discharge capacity keeps almost unchanged after 80 cycles, showing the embedded LMFP-AB/C has good structure stability.

The electrochemical impedance spectroscopy (EIS) was used to understand the effects of embedded AB on the lithium insertion/extraction process in the electrode. The impedance spectra of the fresh cells and the cells cycled for 15 times, obtained at open circuit voltage (3.0 V), are presented in Fig. 5(e) and (f). The spectra show a merged semicircle at high frequencies and a straight line at low frequencies. The former is related to the interface impedance between the active materials and electrolyte, and the latter is related to the diffusion of lithium ions inside the active materials [24–27]. The diameter of the semicircle is the interface resistance including the resistance of charge transfer and solid electrolyte interphase, while the slope of the straight line is proportional to the diffusion coefficient of lithium ion (D_{Li}). For the fresh cell (Fig. 5(e)), LMFP-AB/C shows smaller interface resistance and faster diffusion of lithium ion than LMFP/C, which can be ascribed to the porous structure of LMFP-AB/C. After cycling, the interface resistance becomes smaller for both electrodes and less difference exists between two electrodes (Fig. 5(f)), which can be ascribed to the improved contact area between active materials and electrolyte. On the other hand, the difference in diffusion kinetics of lithium ion is still observed between two electrodes, suggesting that the inside structure of LMFP-AB/C is different from that of LMFP/C and keeps unchanged after cycling. Therefore, the embedded AB provides $LiMn_{0.8}Fe_{0.2}PO_4$ with large specific surface area and improves lithium ion diffusion inside $LiMn_{0.8}Fe_{0.2}PO_4$.

4. Conclusions

We reported a novel $LiMn_{0.8}Fe_{0.2}PO_4$/C composite, acetylene black embedded $LiMn_{0.8}Fe_{0.2}PO_4$, as cathode material of lithium ion battery. The embedded porous carbon provides not only the electronic conductive network due to the good electronic conductivity of acetylene black, but also the ionic paths due to its porous structure. With these characteristics, the resulting $LiMn_{0.8}Fe_{0.2}PO_4$/C composite exhibits the improved performance compared with the composite without acetylene black embedded.

Acknowledgments

This work is supported by the joint project of National Natural Science Foundation of China and Natural Science Foundation of Guangdong Province (Grant No. U1134002), National Natural Science Foundation of China (Nos. 21003054 and 21273084), Natural Science Fund of Guangdong Province (Grant Nos. 10351063101000001 and S2011040001731), and key project of Guangdong Province (Grant No. 20110110).

References

[1] Z.P. Cai, Y. Liang, W.S. Li, L.D. Xing, Y.H. Liao, J. Power Sources 189 (2009) 547–551.
[2] B. Kang, G. Ceder, Nature 458 (2009) 190–193.
[3] S.-Y. Chung, J.-G. Kim, Y.-M. Kim, Y.-B. Lee, Adv. Mater. 23 (2011) 1398–1403.
[4] G. Kobayashi, S.-i . Nishimura, M.-S. . Park, R. Kanno, M. Yashima, T. Ida, A. Yamada, Adv. Funct. Mater. 19 (2009) 395–403.
[5] Y. Wang, J. Wang, J. Yang, Y. Nuli, Adv. Funct. Mater. 16 (2006) 2135–2140.
[6] S.-M. Oh, S.-W. Oh, C.-S. Yoon, B. Scrosati, K. Amine, Y.-K. Sun, Adv. Funct. Mater. 20 (2010) 3260–3265.
[7] S.K. Martha, B. Markovsky, J. Grinblat, Y. Gofer, O. Haik, E. Zinigrad, D. Aurbach, T. Drezen, D. Wang, G. Deghenghi, I. Exnar, J. Electrochem. Soc. 156 (2009) A541–A552.
[8] Z. Bakenov, I. Taniguchi, Electrochem. Commun. 12 (2010) 75–78.
[9] G. Chen, T.J. Richardson, J. Power Sources 195 (2010) 1221–1224.
[10] D. Choi, D. Wang, I.T. Bae, J. Xiao, Z. Nie, W. Wang, V.V. Viswanathan, Y.J. Lee, J.G. Zhang, G.L. Graff, Z. Yang, J. Liu, Nano Lett. 10 (2010) 2799–2805.
[11] M. Pivko, M. Bele, E. Tchernychova, N.Z. Logar, R. Dominko, M. Gaberscek, Chem. Mater. 24 (2012) 1041–1047.
[12] S.K. Martha, J. Grinblat, O. Haik, E. Zinigrad, T. Drezen, J.H. Miners, I. Exnar, A. Kay, B. Markovsky, D. Aurbach, Angew. Chem. Int. Ed. 48 (2009) 8559–8563.
[13] J. Hong, F. Wang, X. Wang, J. Graetz, J. Power Sources 196 (2011) 3659–3663.
[14] K. Saravanan, V. Ramar, P. Balaya, J.J. Vittal, J. Mater. Chem. 21 (2011) 14925–14935.
[15] H. Wang, Y. Yang, Y. Liang, L.-F. Cui, H. Sanchez Casalongue, Y. Li, G. Hong, Y. Cui, H. Dai, Angew. Chem. Int. Ed. 50 (2011) 7364–7368.
[16] Y. Zhang, C.S. Sun, Z. Zhou, Electrochem. Commun. 11 (2009) 1183–1186.
[17] Y. Wang, Y. Wang, E. Hosono, K. Wang, H. Zhou, Angew. Chem. Int. Ed. 47 (2008) 7461–7465.
[18] A. Pan, J. Liu, J.-G. Zhang, W. Xu, G. Cao, Z. Nie, B.W. Arey, S. Liang, Electrochem. Commun. 12 (2010) 1674–1677.
[19] S.W. Oh, S.-T. Myung, S.-M. Oh, K.H. Oh, K. Amine, B. Scrosati, Y.-K. Sun, Adv. Mater. 22 (2010) 4842–4845.
[20] H. Yoo, M. Jo, B.-S. Jin, H.-S. Kim, J. Cho, Adv. Energy Mater. 1 (2011) 347–351.
[21] L. Zhang, H. Xiang, Z. Li, H. Wang, J. Power Sources 203 (2012) 121–125.
[22] L. Zhao, Y.-S. Hu, H. Li, Z. Wang, L. Chen, Adv. Mater. 23 (2011) 1385–1388.
[23] A.F. Liu, Z.B. Wen, Y.F. Liu, Z.H. Hu, Funct. Mater. Lett. 4 (2011) 319–322.
[24] K. Yang, X. Hu, Y. Huai, Z. Shi, Z. Deng, J. Suo, J. Solid State Electrochem 16 (2012) 1055–1065.
[25] D. Aurbach, J. Power Sources 89 (2000) 206–218.
[26] D.S. Lu, W.S. Li, X.X. Zuo, Z.Z. Yuan, Q.M. Huang, J. Phys. Chem. C 111 (2007) 12067–12074.
[27] R.H. Zeng, W.S. Li, D.S. Lu, Q.M. Huang, J. Power Sources 174 (2007) 592–597.